



MRI evaluation of soft tissue tumors: comparison of a fast, isotropic, 3D T2-weighted fat-saturated sequence with a conventional 2D T2-weighted fat-saturated sequence for tumor characteristics, resolution, and acquisition time

Rodrigo de Castro Luna¹ · Neil M. Kumar¹ · Jan Fritz² · Shivani Ahlawat¹ · Laura M. Fayad¹

Received: 15 February 2022 / Revised: 24 May 2022 / Accepted: 30 May 2022 / Published online: 25 June 2022
© The Author(s), under exclusive licence to European Society of Radiology 2022

Abstract

Objectives To test whether a 4-fold accelerated 3D T2-weighted (T2) CAIPIRINHA SPACE TSE sequence with isotropic voxel size is equivalent to conventional 2DT2 TSE for the evaluation of intrinsic and perilesional soft tissue tumors (STT) characteristics.

Methods For 108 patients with histologically-proven STTs, MRI, including 3DT2 (CAIPIRINHA SPACE TSE) and 2DT2 (TSE) sequences, was performed. Two radiologists evaluated each sequence for quality (diagnostic, non-diagnostic), tumor characteristics (heterogeneity, signal intensity, margin), and the presence or absence of cortical involvement, marrow edema, and perilesional edema (PLE); tumor size and PLE extent were measured. Signal-to-noise (SNR) and contrast-to-noise (CNR) ratios and acquisition times for 2DT2 in two planes and 3DT2 sequences were reported. Descriptive statistics and inter-method agreement were reported.

Results Image quality was diagnostic for all sequences (100% [108/108]). No difference was observed between 3DT2 and 2DT2 tumor characteristics ($p < 0.05$). There was no difference in mean tumor size (3DT2: 2.9 ± 2.5 cm, 2DT2: 2.8 ± 2.6 cm, $p = 0.4$) or PLE extent (3DT2: 0.5 ± 1.2 cm, 2DT2: 0.5 ± 1.0 cm, $p = 0.9$) between the sequences. There was no difference in the SNR of tumors, marrow, and fat between the sequences, whereas the SNR of muscle was higher ($p < 0.05$) on 3DT2 than 2DT2. CNR measures on 3DT2 were similar to 2DT2 ($p > 0.1$). The average acquisition time was shorter for 3DT2 compared with 2DT2 (343 ± 127 s vs 475 ± 162 s, respectively).

Conclusion Isotropic 3DT2 MRI offers higher spatial resolution, faster acquisition times, and equivalent assessments of STT characteristics compared to conventional 2DT2 MRI in two planes. 3DT2 is interchangeable with a 2DT2 sequence in tumor protocols.

Key Points

- *Isotropic 3DT2 CAIPIRINHA SPACE TSE offers higher spatial resolution than 2DT2 TSE and is equivalent to 2DT2 TSE for assessments of soft tissue tumor intrinsic and perilesional characteristics.*
- *Multiplanar reformats of 3DT2 CAIPIRINHA SPACE TSE can substitute for 2DT2 TSE acquired in multiple planes, thereby reducing the acquisition time of MRI tumor protocols.*
- *3DT2 CAIPIRINHA SPACE TSE and 2DT2 TSE had similar CNR of tissues.*

Keywords CAIPIRINHA · Magnetic resonance imaging · Soft tissue tumors · SPACE · Three-dimensional

✉ Laura M. Fayad
lfayad1@jhmi.edu

¹ Russell H. Morgan Department of Radiology and Radiological Science, Johns Hopkins Hospital/The Johns Hopkins Medical Institutions, 600 North Wolfe Street, Baltimore, MD 21287, USA

² New York University Grossman School of Medicine, New York University, New York, NY, USA

Abbreviations

2D	Two dimensional
3D	Three dimensional
ADC	Apparent diffusion coefficient
CAIPIRINHA	Controlled Aliasing in Parallel Imaging Results in Higher Acceleration
CNR	Contrast-to-noise ratio

DWI	Diffusion-weighted MR imaging
FOV	Field-of-view
FSE	Fast spin-echo
IW	Intermediate weighted
MRI	Magnetic resonance imaging
PACS	Picture archiving and communication system
ROI	Region of interest
SI	Signal intensity
SNR	Signal-to-noise ratio
SPACE	Sampling perfection with application-optimized contrasts using different flip angle evolution
SPAIR	Spectral adiabatic inversion-recovery
SPIR	Spectral presaturation with inversion recovery
TE	Echo time
TR	Repetition time
TSE	Turbo spin echo
TWIST	Time-resolved angiography with interleaved stochastic trajectories
VIBE	Volume intercalated breathhold exam
W	Weighted

Introduction

Fast magnetic resonance imaging (MRI) protocols using three-dimensional (3D) isotropic turbo spin-echo (TSE) sequences have been developed for the evaluation of internal joint derangement [1–15] and recently, for the assessment of bone tumor extent with 3D T1-weighted imaging [16]. The isotropic voxel size of 3D sequences with high spatial resolution allows reformatting of MR images in any desired orientation and slice thickness following a single parental MRI acquisition, a means of providing fast imaging.

The contrast resolution, multiplanarity, and acquisition time of three-dimensional TSE sequences utilizing Sampling Perfection with Application optimized Contrasts using different flip-angle Evolution (SPACE) have been improved by incorporating optimized bi-directional parallel imaging, specifically with the use of Controlled Aliasing in Parallel Imaging Results in Higher Acceleration (CAIPIRINHA) sampling patterns [17]. While the diagnostic performance of 3D CAIPIRINHA SPACE sequences using intermediate- and T2-weighted contrast is equivalent to or better than that of standard 2D TSE in joints [3, 6, 7, 11], nerves [18], and spine [19, 20], the validation of a 3D T2-weighted fat-saturated sequence for soft tissue tumor (STT) evaluation, which requires precise evaluation of internal signal composition and peri-tumoral signal [21], has not been previously shown, to our knowledge. Recently, a dedicated isotropic 3D T1-weighted CAIPIRINHA SPACE sequence for bone tumor evaluation

was shown to be equivalent to 2D T1-weighted TSE for assessing intramedullary bone tumor extent and bone tumor characteristics [16].

Fat-suppressed 2D T2-weighted TSE is an essential sequence for the assessment of STTs. However, 2D T2-weighted TSE is limited by anisotropic voxels, with relatively thick image sections. Typically, multiple separate acquisitions of 2D TSE sequences in different planes are performed to assess STTs, contributing to longer acquisition times of MRI tumor protocols [14, 22–26]. We hypothesized that a dedicated volumetric 3D T2 sequence with isotropic voxel size and contrast resolution similar to standard 2D TSE could provide higher spatial resolution, virtually infinite multiplanarity, at least equivalent STT assessments, and shorter MRI protocol times. Therefore, the purpose of our study was to test whether a 4-fold accelerated 3DT2 CAIPIRINHA SPACE sequence with isotropic voxel size offers at least equivalent performance compared to conventional 2DT2 TSE for the evaluation of intrinsic and perilesional STT characteristics.

Materials and methods

Study design

Our institutional review board approved this retrospective single-center study, which was performed in compliance with both the Declaration of Helsinki and Health Insurance Portability and Accountability Act (HIPPA) regulations. The requirement for informed consent was waived.

Inclusion criteria were patients with STTs with histopathologic confirmation by percutaneous biopsy or surgical specimen, who underwent MRI on a 3-Tesla (3T) system, which included both fat-suppressed 3DT2 and 2DT2 sequences, between March 2017 and September 2020, prior to treatment. Exclusion criteria were patients with incomplete imaging. The study design is shown in Figure 1.

MRI acquisition

All MRI studies were performed on a commercially available clinical wide-bore 3-T MRI system (Magnetom Skyra, Siemens Healthcare) with a gradient strength of 45 mT/m and a slew rate of 200 mT/m/ms. Different multichannel surface coils were used depending on the anatomic site, including the trunk and extremities. The MRI protocol included a fat-suppressed anisotropic 2D TSE sequence with separate acquisitions in at least two planes and a fat-suppressed 3D CAIPIRINHA SPACE TSE sequence with isotropic voxel resolution and a dedicated flip angle modulation scheme to create T2 contrast (Table 1). Our institutional MRI protocol also included T1-weighted imaging with and without contrast, with dynamic contrast-enhanced MR, chemical shift imaging,

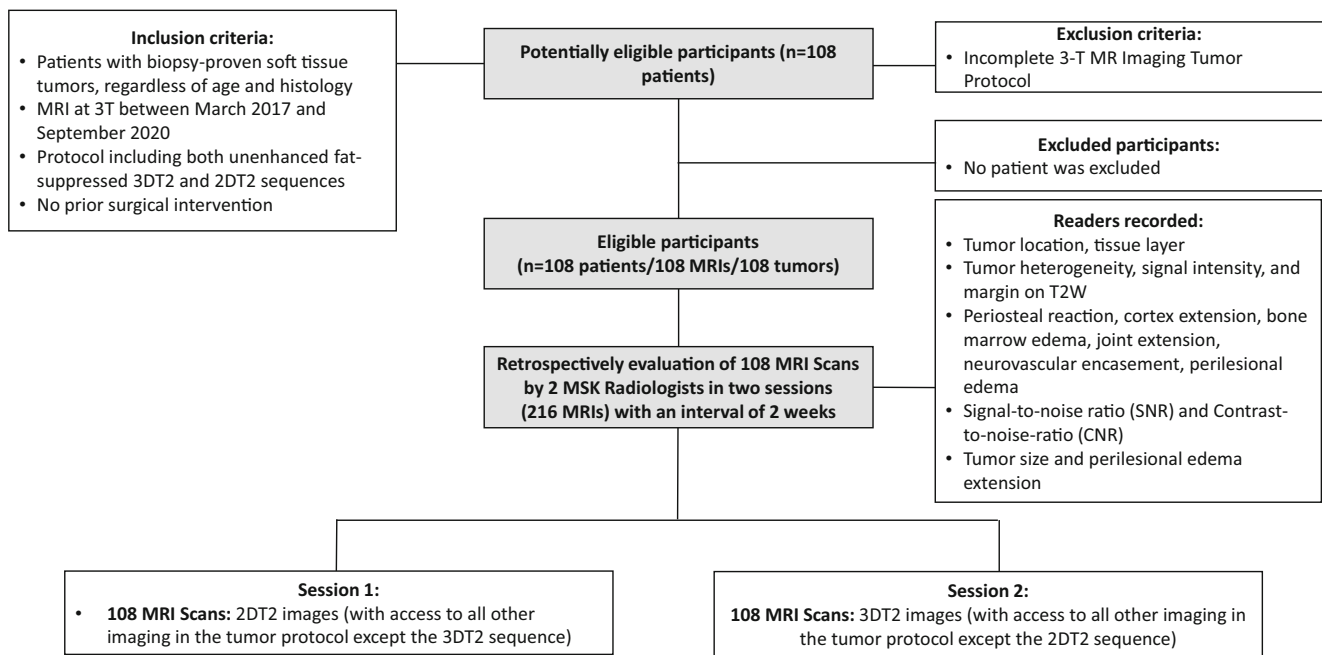


Fig. 1 Study flow diagram

and diffusion-weighted imaging. The matrix and field of view (FOV) varied by anatomic site.

Image analysis

All anonymized MRI studies were reviewed separately by two musculoskeletal radiologists (with 16 and 10 years of clinical experience) in random order. The two readers assessed the

MRI exams in two separate interpretation sessions. First, the readers reviewed the 2DT2 images (along with all other imaging in the tumor protocol except the 3DT2 sequence), and in a second session at least two weeks later, readers reviewed the 3DT2 images (along with all other imaging in the tumor protocol except the 2DT2 sequence). The images were digitally assessed using a commercially available picture archiving and communication system (PACS) workstation (Carestream

Table 1 MR imaging parameters

Parameters	2DT2 TSE	3DT2 CAIPIRINHA SPACE
Orientation	Axial/coronal	Coronal/sagittal
Repetition time (msec)	3500–5750	950–1100
Echo time (msec)	57–74	102–108
Acceleration factor	2	2
Echo train length	14–16	42
Receiver bandwidth (Hz/pixel)	200–250	347–425
Flip angle (degree)	150	120
Acquisition matrix	192–512 × 132–416	256–320 × 256–320
Slice thickness (mm)	2.5–6	0.6–1
Intersection gap (mm)	0.2–0.6	0
Number of Slices	32–45	160–240
Reconstructed voxel size (mm)	0.3–0.6 × 0.3–0.6 × 2.5–6.0	0.6–1.0 × 0.6–1.0 × 0.6–1.0
Voxel volume (mm ³)	0.7–1.8	0.2–1
No. excitations	2	1
Phase encoding direction	Right to left / right to left	Right to left / anterior to posterior
Fat suppression	Fat sat. / SPAIR	SPAIR
Time of acquisition	475 s (± 162 s, range 332–750 s) (for 2 planes)	343 s (± 127 s, range 184–516 s)

MR indicates magnetic resonance; 2D, 2-dimensional; 3D, 3-dimensional; FS, fat-suppressed; SPAIR, Spectral Attenuated Inversion Recovery

Health Inc., Canada). The readers viewed the data sets in interactive multiplanar reconstruction mode with preferred window, magnification, and scrolling settings. At the time of analysis, the readers had no access to medical records and did not know clinical history, histopathological examination results, or previous MR reports.

Overall subjective image quality for 2DT2 and 3DT2 sequences was rated on a semiquantitative scale (1 = nondiagnostic, with artifacts involving > 50% of the images, 2 = diagnostic, with artifacts involving 25%–50 % of the images, 3 = diagnostic, but with artifacts involving < 25% of the images, 4 = diagnostic, with no appreciable artifacts). Artifacts were reported as motion-related, due to failure of fat-suppression or loss of signal not otherwise specified.

Readers recorded the tumor anatomic location (pelvic, thigh, leg/calf, knee, foot, arm, forearm, elbow, wrist/hand or shoulder/axilla), tissue layer (subcutaneous, intramuscular, intermuscular, intra-articular or mixed), and tumor characteristics, including heterogeneity (homogeneous, < 25% heterogeneous, 25–75% heterogeneous or > 75% heterogeneous), predominant signal intensity (isointense, hypointense, or hyperintense to muscle), and tumor margin (poorly defined = > 75% of margin not clear, mixed definition = 10–25% of margin not clear, or well defined = > 90% of margin clear). Readers also recorded the presence or absence of periosteal reaction, cortical extension, bone marrow signal, intra-articular extension, neurovascular encasement, and perilesional soft-tissue edema, according to the definitions below. Both readers independently measured the tumor size (largest tumor length) and, if any, the peritumoral edema extent (largest linear extent).

The presence of periosteal reaction was reported when there was a change in signal intensity and or displacement and or thickening of the periosteum. Cortex extension was defined as contact between tumor and bone with associated changes in cortical signal intensity. Mere contact without signal alterations was not considered a sign of invasion [27]. High T2 signal with a vague margin and with decreased signal intensity on the opposed phase image compared with the in-phase was considered an indicator of bone marrow edema or red marrow, while preserved signal in the opposed phase compared with in-phase imaging was considered an indicator of tumor infiltration of the bone marrow [23]. Intra-articular extension was defined as the presence of tumor within the synovial membrane border. Encasement of arteries, veins, and nerves was diagnosed if the contact between tumor and vascular or neural circumference exceeded 180° [28]. Peritumoral edema was defined as regions of hyperintense T2 signal contiguous to and surrounding the tumor margin/pseudocapsule.

SNR and CNR measurements were made on 2DT2 and 3DT2 sequences by one reader, with regions of interest (ROIs) of the tumor, bone marrow, subcutaneous fat, and

muscle. In order to minimize a potential error on the SNR estimate, round or oval ROIs (region of interest) were copied into identical sizes and locations on 2D and 3D MR images, and the region of interest areas was approximately 15–20 mm² for cancellous bone, subcutaneous fat, muscle, and background (air). A circular or elliptical ROI was drawn to include the most considerable portions of the tumors, and the SI_{tumor} was recorded. The mean pixel value was used as the signal intensity, and the standard deviation (SD) of background ROI was used as the noise. The reader was careful to avoid regions that might contain motion artifacts (ghosting and ringing), a region of inhomogeneous fat suppression, or large blood vessels. The SNR was determined as the ratio of the mean signal intensity of tissue to the standard deviation of the signal in an ROI placed in the background (SNR: $SI/SD_{\text{background}}$). Although this method can be prone to geometry factor-based SNR estimate errors, it is the only method to retrospectively assess SNR, and we placed the background ROI as proximal to the tumor signal ROI as possible to minimize errors related to the spatial variance of noise [29]. Tumor conspicuity (CNR_{tumor}) against the background of skeletal muscle, cancellous bone, or subcutaneous fat was calculated by using the formula: $CNR_{\text{tumor}} = SNR_{\text{tumor}} - SNR_{\text{skeletal muscle, muscle, or subcutaneous fat}}$ [30].

The acquisition time of the 2DT2 and 3DT2 sequences was recorded by one reader for each patient and was obtained from the Digital Imaging and Communications in Medicine document associated with each MRI.

Statistical analysis

Statistical analyses were performed using Matlab software (R2019a, The MathWorks). Descriptive statistics were reported. The average acquisition times for 2D and 3D imaging were compared using a Wilcoxon signed-rank test for non-parametric paired data. The inter-method concordance was defined as the degree of agreement between 2D and 3D studies to evaluate intrinsic and perilesional soft tissue tumor characteristics and was assessed with Wilcoxon Rank and Cohen kappa tests. The tumor size and peritumoral edema extent on 2D and 3D sequences were compared using a paired Student *t*-test. A paired Student *t*-test was used to compare SNR and CNR between sequences. Intraclass correlation coefficient (ICC) was used to calculate absolute agreement for single measurements for both tumor size and peritumoral edema extension [31]. The 95 % confidence intervals (CIs) associated with the ICCs were also calculated. Agreement was interpreted as poor agreement (ICC, 0–0.2), fair agreement (ICC, 0.3–0.4), moderate agreement (0.5–0.6), strong agreement (ICC, 0.7–0.8), or excellent agreement (ICC, > 0.8). Statistical significance was assumed for $p < 0.05$.

Results

There were 108 STTs included and Table 2 lists their characteristics. The population consisted of 60/108 (55.6%) women and 48/108 (44.4%) men with a mean age of 46.2 years (\pm 18.8 years, range 11–87 years). Tumors were present in the subcutaneous layer (71/108, 65.7%) and deeper tissues (intramuscular, intermuscular, intra-articular, or mixed) (37/108, 34.3%). Lesion histologies included malignant lesions including primary sarcomas, lymphoma, and metastatic malignancies, and benign entities such as nerve sheath tumors, vascular malformations, and desmoid tumors.

For the evaluation of subjective image quality, 3DT2 and 2DT2 sequences were similarly rated as diagnostic by the two readers (reader 1:100% [108/108] vs reader 2: 99.1% [107/108]), with the majority fitting into the categories “no artifact” or “diagnostic with mild artifact (1–25% artifact)” on both sequences (3DT2: reader 1, 95.4% [103/108] and reader 2, 93.5% [101/108] vs 2DT2: reader 1, 100% [108/108] and reader 2, 97.2% [105/108]). However, a significantly higher number of cases were rated as “diagnostic with mild artifact” on 3DT2 (29.6% [32/108]) compared with 2DT2 (7.4% [8/108]). Table 3 summarizes intrinsic and perilesional STT

characteristics on 2DT2 and 3DT2 protocols, as well as results for the inter-method agreement. No significant difference was observed between the MRI sequences for all tumor characteristics evaluated by the two readers ($p > 0.05$). Tumors were mostly heterogeneous and predominantly hyperintense, without statistical difference between 2D and 3D methods ($p > 0.05$). Tumor margins were mostly well-defined rather than mixed definition or poorly defined. There was no significant difference between the sequences ($p > 0.05$) in the determination of the presence of cortex extension and bone marrow edema, joint extension, neurovascular encasement, and perilesional edema (Figures 2 and 3), as well as in the determination of the tissue layer involved by perilesional edema.

There was no significant difference in the measurements of tumor size between 3DT2 and 2DT2 ($p = 0.4$), with the mean largest size of 2.9 ± 2.5 cm (range 0.3–19 cm) on 3DT2 and 2.8 ± 2.6 cm (range 0.3–18.2 cm) on 2DT2 sequences. Likewise, there was no difference in the measurement of perilesional edema ($p = 0.9$) on 3DT2 (0.5 ± 1.2 cm, range 0.2–7 cm) or 2DT2 (0.5 ± 1.0 cm, range 0.3–6.3 cm) sequences (Figure 4). Inter-reader reliability was excellent for tumor size measurements (ICC 0.9–1.0) and was strong for measuring perilesional edema made by the readers on 3D and 2D sequences (ICC 0.7).

Table 2 Characteristics of subjects

Tumors	108
Age [year] (standard deviation)	46.2 \pm 18.8
Female sex	60/108 (55.5%)
Tumor location	
Upper extremities	55/108 (50.9%)
Lower extremities	40/108 (37%)
Pelvis	13/108 (12%)
Tumor location (tissue layer)	
Subcutaneous	70/108 (64.8%)
Intramuscular	15/108 (13.9%)
Intermuscular	10/105 (9.3%)
Mixed	9/108 (8.3%)
Intra-articular	4/108 (3.7%)
Bening tumors	95/108 (88%)
Malignant tumors	13/108 (12%)
Histology	18/108 (16.7%) Desmoid, fibromatosis, fibronodular fasciitis, Morton’s neuroma 15/108 (13.9%) lipoma 13/108 (12%) pigmented villonodular synovitis, giant cell tumor of tendon sheath 12/108 (11.1%) Ganglion, mucous cysts 10/108 (9.2%) sarcoma 9/108 (8.3%) neurofibroma, schwannoma 5/108 (4.6%) glomus tumor, 2/108 (1.8%) metastases, 24/108 (22.2%) other

Table 3 Intrinsic and perilesional STT characteristics on each sequence and inter-method agreement

Parameters	Reader 1			Reader 2		
	2DT2	3DT2	Inter-method agreement <i>p</i> values*	2DT2	3DT2	Inter-method agreement <i>p</i> values*
Tissue layer						
Subcutaneous	70/108 (64.8%)	71/108 (65.7%)	0.8	66/108 (61.1%)	64/108 (59.3%)	0.8
Intramuscular	15/108 (13.9%)	16/108 (14.8%)		17/108 (15.7%)	17/108 (15.7%)	
Intermuscular	10/108 (9.3%)	11/108 (10.2%)		11/108 (10.2%)	12/108 (11.1%)	
Intra-articular	4/108 (3.7%)	4/108 (3.7%)		5/108 (4.6%)	5/108 (4.6%)	
Mixed	9/108 (8.3%)	6/108 (5.6%)		9/108 (8.3%)	10/108 (9.3%)	
Heterogeneity on T2W						
Homogeneous	27/108 (25%)	28/108 (25.9%)	0.6	27/108 (25%)	26/108 (24.1%)	0.7
< 25% heterogeneous	42/108 (38.9%)	36/108 (33.3%)		27/108 (25%)	34/108 (31.5%)	
25–75% heterogeneous	35/108 (32.4%)	38/108 (35.2%)		47/108 (43.5%)	40/108 (37%)	
> 75% heterogeneous	4/108 (3.7%)	6/108 (5.6%)		7/108 (6.5%)	8/108 (7.4%)	
Signal intensity on T2W						
Hyperintense	79/108 (73.1%)	81/108 (75%)	0.8	76/108 (70.4%)	78/108 (72.2%)	0.7
Hypointense	25/108 (23.2%)	25/108 (23.1%)		27/108 (25%)	28/108 (25.9%)	
Isointense	4/108 (3.7%)	2/108 (1.9%)		5/108 (4.6%)	2/108 (1.8%)	
Tumor margin on T2W						
Well defined (> 90% of margin clear)	84/108 (77.8%)	86/108 (79.6%)	0.6	84/108 (77.8%)	84/108 (77.8%)	0.9
Mixed definition (10–25% of margin not clear)	14/108 (13%)	13/108 (12.1%)		11/108 (10.2%)	12/108 (11.1%)	
Poorly defined (> 75% of margin not clear)	10/108 (9.2%)	9/108 (8.3%)		13/108 (12%)	12/108 (11.1%)	
Cortical extension	4/108 (3.7%)	4/108 (3.7%)	1	5/108 (4.6%)	2/108 (1.8%)	0.3
Bone marrow edema	5/108 (4.6%)	4/108 (3.7%)	0.7	7/108 (6.5%)	2/108 (1.8%)	0.1
Intra-articular extension	7/108 (6.5%)	7/108 (6.5%)	1	6/108 (5.6%)	7/108 (6.5%)	0.8
Neurovascular encasement	6/108 (5.6%)	5/108 (4.6%)	0.7	1/108 (0.9%)	2/108 (1.8%)	0.6
Perilesional edema- tissue layer						
Subcutaneous	19/108 (17.6%)	19/108 (17.6%)	0.9	34/108 (31.5%)	33/108 (30.6%)	0.2
Intramuscular	7/108 (6.5%)	6/108 (5.6%)		8/108 (7.4%)	6/108 (5.6%)	
Intermuscular	1/108 (0.9%)	2/108 (1.8%)		9/108 (8.3%)	6/108 (5.6%)	
Mixed	4/108 (3.7%)	4/108 (3.7%)		16/108 (14.8%)	12/108 (11.1%)	
Absent	77/108 (71.3%)	77/108 (71.3%)		41/108 (37.8%)	51/108 (47.2%)	

*Wilcoxon rank test

SNR and CNR analyses are given in Table 4. The SNR measures in the tumors, bone marrow, and fat were not significantly different between 3DT2 and 2DT2 images, whereas the SNR of muscle was significantly higher ($p < 0.05$) in 3DT2 images (3DT2 = 95.3 ± 55.3 [range, 10.7–285.9] vs 2DT2: 68.3 ± 43.8 [range, 11.2–300.6]). The conspicuity of STTs on 3DT2 assessed through CNR against the background of bone marrow, muscle, and fat showed statistically similar results compared with measurements obtained from 2DT2 sequences ($p > 0.05$) (Figure 5).

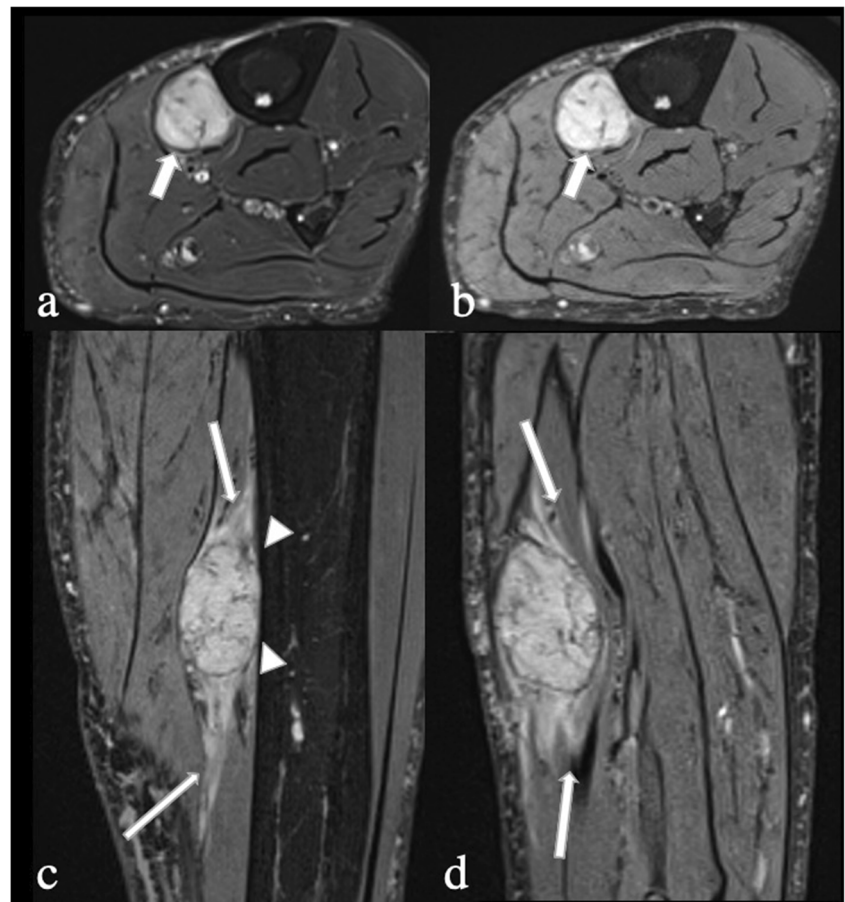
All the MR examinations were performed on a 3-T system, and the 3DT2 sequence required an average acquisition time of 343 s (± 127 s, range 184–516 s) (average acquisition time of 184, 266, 407, and 516 s for wrist/hand,

foot, leg/arm/forearm/thigh, and pelvis, respectively), while two plane 2DT2 sequences (coronal and axial) had an average acquisition time of 475 s (± 162 s, range 332–750 s) (average acquisition time of 396, 332, 420, and 750 s for wrist/hand, foot, leg/arm/forearm/thigh, and pelvis, respectively).

Discussion

Our investigation showed that an isotropic 3DT2 SPACE sequence with CAIPIRINHA acceleration at 3T provides equivalent STT contrast resolution and diagnostic lesion assessment compared to conventional 2DT2 TSE sequences. An isotropic

Fig. 2 Malignant epithelioid neoplasm within flexor digitorum longus muscle in a 75-year-old man (arrow). **a** Axial fat-suppressed 2D T2W TSE (TR, 4100 ms; TE, 78 ms) and multiplanar reformations in **(b)** axial, **(c)** coronal, and **(d)** sagittal planes from high-resolution fat-suppressed 3D SPACE T2W (TR, 1000 ms; TE, 103 ms) show good contrast resolution between mass and surrounding muscle in both techniques, and comparable intrinsic and perilesional soft tissue tumor characteristics between 2D and 3D techniques (mass with heterogeneous signal intensity, predominantly hyperintense signal with central hypointense septae, and perilesional edema (long arrow)). Coronal reconstructed 3-mm 3D SPACE image clearly depicts that the mass abuts the posterior medial cortex of the tibia, but with no signs of infiltration (arrowheads)



3DT2 sequence with multiplanar reformatting capabilities can replace separately acquired 2DT2 sequences in two planes, with the added benefit of shorter acquisition times.

Although most current TSE-based 2D sequences have high spatial resolution, provide a variety of image contrasts, and are resistant to image artifacts from radio-frequency (RF) and

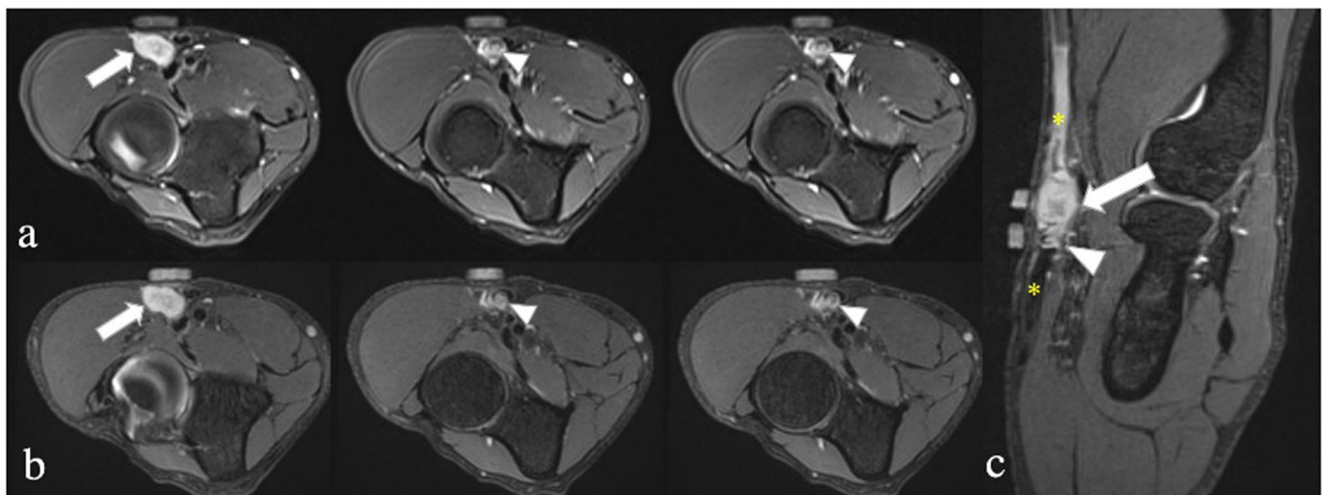


Fig. 3 Subcutaneous fascia-based nodular fasciitis in the antecubital fossa (arrow) of a 43-year-old man, with intravascular extension in the cephalic vein (arrowheads). **a** Fat-suppressed 2D T2W TSE (TR, 3360 ms; TE, 56 ms) and **(b)** 3D SPACE T2W (TR, 950 ms; TE, 108 ms) consecutive images in axial plane showing a well-defined 1.8 x 1.4 x 0.9 cm hyperintense nodule (arrow), medial to the brachioradialis,

superficial to the biceps tendon, and indistinct from the cephalic vein, presenting intraluminal component (arrowheads) characterized by partial replacement of signal void by the tumor, more evident in the 3D sequence. **c** Curved planar reformation image of the cephalic vein (asterisk) from 3D SPACE T2W revealing the intravascular extension of the nodule (arrowheads), later confirmed by histopathological analysis

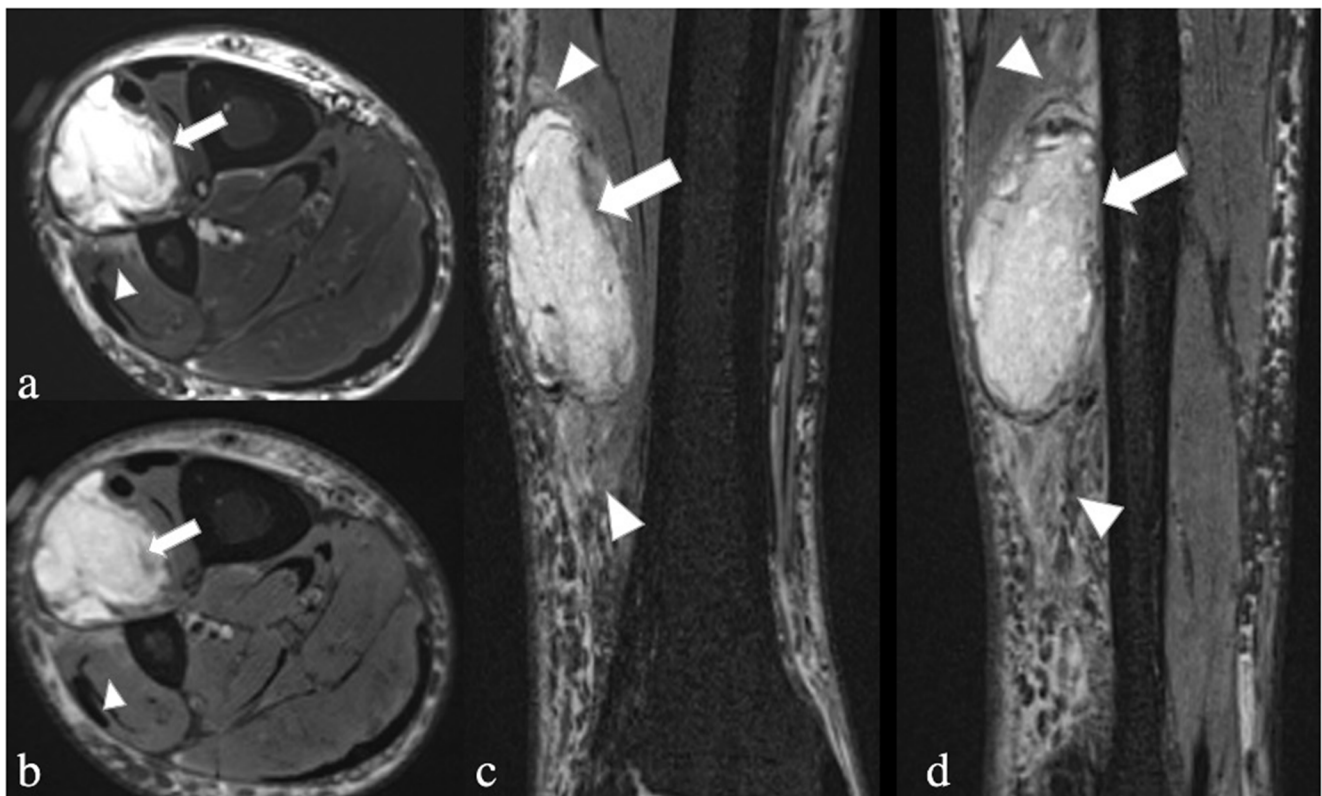


Fig. 4 Images of a 75-year-old man with grade 3 deep intramuscular sarcoma (undifferentiated pleomorphic sarcoma). The MR images show features of a high-grade tumor, including internal signal intensity heterogeneity, perilesional abnormalities, and large size (3.5 × 3.0 × 7.4 cm). **a** Fat-suppressed Axial 2D T2W TSE (TR, 4200 ms; TE, 78 ms) and **(b)** axial, **(c)** sagittal, and **(d)** coronal reformations from high-resolution

fat-suppressed 3D SPACE T2W (TR, 1000 ms; TE, 103 ms) show a heterogeneously hyperintense mass replacing the extensor digitorum longus muscle (arrow) with surrounding myofascial and subcutaneous perilesional edema (arrowheads), similarly depicted in both techniques (2D and 3D)

static field inhomogeneity, they have limitations such as relatively thick image sections and anisotropic voxels. Therefore, tumor assessment with 2D imaging requires a separate

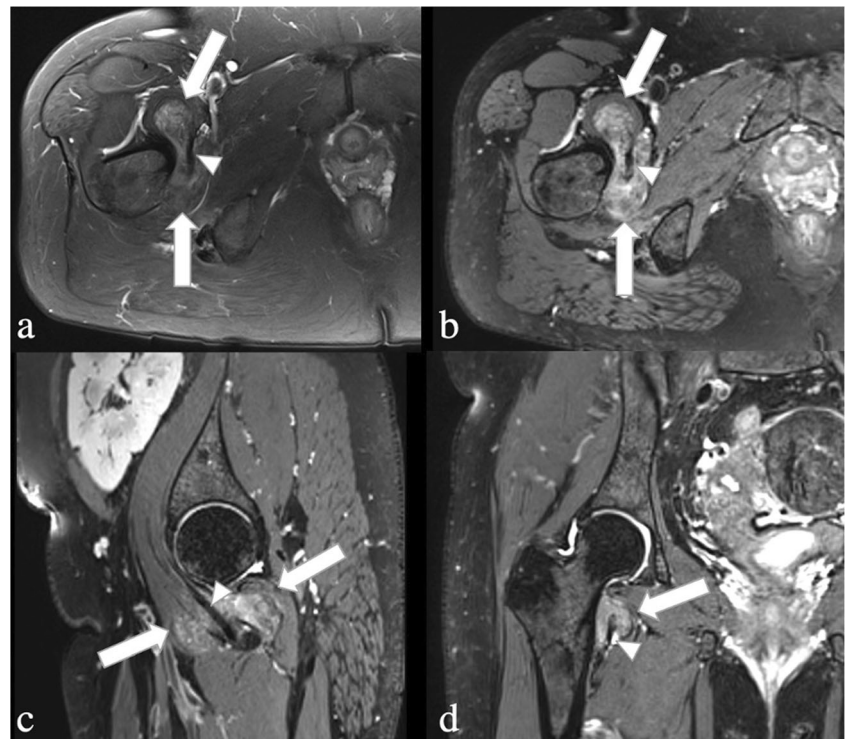
acquisition for every desired image plane, increasing the overall examination time. With the advent of high field strength MRI systems, high-performance gradients, dedicated

Table 4 Signal-to-noise ratio (SNR) and Contrast-to-noise ratio (CNR)

Parameters		2D T2FS	3D T2FS	<i>p</i> value*
Signal-to-noise ratio	Tumor	165.4 ± 180.3 (3.2–1355.8)	174 ± 163.4 (9.4–911.6)	0.6
	Bone marrow	38.1 ± 30.2 (3.6–170.9)	38.1 ± 30.2 (5.2–142.3)	1
	Muscle	68.3 ± 43.8 (11.2–300.6)	95.3 ± 55.3 (10.7–285.9)	< 0.05
	Fat	58.1 ± 48.3 (4.7–331.9)	53 ± 36.7 (6–180.5)	0.3
Contrast-to-noise ratio	Tumor to bone marrow	127.3 ± 168 (−51.4 to 1184.8)	136 ± 147.4 (−41 to 812.9)	0.5
	Tumor to muscle	97.1 ± 158.5 (−103.9 to 1055)	78.7 ± 132.1 (−139.3 to 625.8)	0.1
	Tumor to fat	107.4 ± 152.1 (−84 to 1023.9)	121 ± 147.1 (−123.5 to 770.4)	0.3

Data presented as mean ± standard deviation (with the range in parenthesis); *Student’s t-test; SNR was calculated as the mean signal intensity (SI) of regions of interest divided by the standard deviation SI of the background (air); CNR was calculated by using the formula: $CNR = SNR_{Tumor} - SNR_{(bone\ marrow,\ muscle\ or\ fat)}$

Fig. 5 MR images in a 48-year-old man with soft tissue mass (arrows) around the right iliopsoas tendon (arrowheads) consistent with pigmented villonodular synovitis. **a** Axial fat-suppressed 2D T2W TSE (TR, 3770 ms; TE, 74 ms) and multiplanar reformations in **(b)** axial, **(c)** sagittal, and **(d)** coronal planes from high-resolution fat-suppressed 3D SPACE T2W (TR, 1100 ms; TE, 105 ms) showing heterogeneous mass characterized by predominantly hyperintense signal, with central areas of hypointense signal, narrow transition zone, with no perilesional edema. The tumor conspicuity (CNR) was visibly better for 3D images versus 2D images in the background of skeletal muscle ($CNR_{\text{muscle}}, 49 \times 1.3$) and fat ($CNR_{\text{fat}}, 78.6 \times 42.9$)



multichannel coils, and improved postprocessing software, 3D MRI is viable for routine clinical practice [2; 11; 22; 23; 25; 26] and can be acquired with shorter cumulative imaging times compared to two or three separate orthogonal 2D sequences, ranging from 5 to 10 min [3; 6; 7; 9; 11; 16].

Optimized single-slab 3D TSE sequence as SPACE has become a clinically useful option for faster high spatial resolution T2-weighted musculoskeletal imaging. Although no significant differences in tumor characteristics were found between 3DT2 and 2DT2 sequences across all tumors, multiplanar high-resolution 3D evaluation may be especially useful in the evaluation of small tumors, in demonstrating intricate anatomic relationships such as the position of a nerve relative to a schwannoma.

While 3D CAIPIRINHA SPACE has been extensively studied in internal derangement, to our knowledge, this is the first report regarding the use of a fat-suppressed T2-weighted 3D CAIPIRINHA SPACE sequence for the evaluation of soft tissue tumors. Previous studies have shown spatial resolution and time of acquisition advantages with adequate SNR in the ankle, and the clinical effectiveness of 10-min knee 3D CAIPIRINHA SPACE knee protocols (2,4). The translation of 3D CAIPIRINHA SPACE MRI to tumor evaluation, which often requires both anatomic and functional MRI sequences and longer exam times, is important as long exam times may exacerbate motion artifacts and patient anxiety and dissatisfaction [32]. Fat-saturated T2 sequences are of paramount importance in assessing intrinsic and perilesional characteristics of any musculoskeletal tumor. Recently, soft

tissue sarcoma characteristics on T2-weighted MRI have been shown to be independently predictive of tumor grade and patient outcomes [33], and the in vivo validation of 3DT2 relative to conventional 2DT2 sequences is important for confident clinical use. Fat saturation in this study was achieved through spectral adiabatic inversion-recovery (SPAIR). With the SPAIR technique, there is more selective fat suppression, relatively low sensitivity to B1 magnetic inhomogeneity, and improved SNR compared with STIR imaging [21, 34]. SPAIR is a particularly excellent technique to use when a large field of view is needed, such as in the pelvis or thigh [34]. Importantly, SPAIR is well suited for use with CAIPIRINHA 3D SPACE T2-weighted sequences, and its higher SNR relative to STIR may allow higher acceleration factors, which can in turn be traded for higher spatial or contrast resolution [17].

Our investigation showed that there were high inter-method and inter-reader agreement for image quality (including motion artifact) between the 3DT2 and the 2DT2 sequences. While no overall differences were seen in fat saturation failure artifact between the sequences, fat saturation failure was occasionally more prominent with the 3DT2 sequence adjacent to marker placement in superficial tumors. Fat saturation failure with 3D chemical shift-based techniques has been previously reported [35] but did not affect the diagnostic value of sequences in our study. Furthermore, SNR and CNR measures were similar between the 3DT2 and 2DT2 sequences, as shown in prior reports of joint imaging, although the SNR of muscle was higher on the 3DT2 images.

Additionally, there were no significant qualitative and quantitative differences between 3DT2 and 2DT2 images in any of the tumors' intrinsic and perilesional characteristics, including signal intensity, heterogeneity, tumor margin, or the presence or absence of cortex extension, bone marrow edema, joint extension, and neurovascular encasement. Specifically, for the intramuscular tumors, there was no significant difference in perilesional edema detection between 2DT2 and 3DT2 ($p > 0.05$) despite higher SNR of muscle on 3DT2 sequences. While we speculated that poorer resolution on 2DT2 sequences could result in misinterpreting adjacent vessels as perilesional edema, perilesional edema detection and extent and tumor size measurements were similar between the 3DT2 and 2DT2 sequences. Hence, our results indicate that the 3DT2 and 2DT2 sequences are interchangeable regarding the identification of STT imaging features.

In addition to providing high-quality images, using a 3-T system, the 3DT2 sequence required an acquisition time 27.8% shorter than a two-plane 2DT2 sequence (343 vs 475 s). Such results indicate that the 3DT2 CAIPIRINHA SPACE sequence is at least equal to and can replace the 2DT2 TSE sequence in the MRI protocol for the evaluation of STTs.

Our study has limitations. First, the visual analysis may be biased, as the readers were not blinded as to which sequence was being evaluated. The imaging appearance of the 2D and 3D datasets was a characteristic (difference in the number of slices and spatial resolutions) allowing them to recognize the technique. However, the readers independently assessed the 3D- and 2D-datasets, separated by at least two weeks to reduce a potential recall and learning bias. Moreover, the 3DT2 protocol was compared to our institutional standard 2D TSE protocol. Assuming that the MRI protocols vary substantially between institutions, our study's sequences may differ from other established protocols, including their acquisition times and image quality. Furthermore, although motion and fat-suppression failure artifacts were not substantially present in our study, it should be emphasized that a potential disadvantage of the 3D sequence is that those artifacts will affect all plane reformations. In contrast, for 2D acquisitions, artifacts only affect the single, separate plane being imaged. Finally, we compared the acquisition time of a 3DT2 sequence with the acquisition time required for 2DT2 imaging in two planes, but in some centers, only one or three 2D imaging planes may be acquired.

In conclusion, our study demonstrated that an accelerated fat-suppressed 3D CAIPIRINHA SPACE T2 sequence provides comparable assessments of STT characteristics to conventional 2DT2 MRI. The isotropic volume acquisition and multiplanar reformation capability of the 3DT2 datasets can replace 2DT2 TSE acquisitions in multiple planes and reduce overall MRI acquisition time.

Funding The authors state that this work has not received any funding.

Declarations

Guarantor The scientific guarantor of this publication is Laura Fayad.

Conflict of interest The authors of this manuscript declare relationships with the following companies: SIEMENS AG.

Statistics and biometry No complex statistical methods were necessary for this paper.

Informed consent Written informed consent was waived by the Institutional Review Board.

Ethical approval Institutional Review Board approval was obtained.

Methodology

- retrospective
- observational
- performed at one institution

References

1. Altahawi FF, Blount KJ, Morley NP, Raithel E, Omar IM (2017) Comparing an accelerated 3D fast spin-echo sequence (CS-SPACE) for knee 3-T magnetic resonance imaging with traditional 3D fast spin-echo (SPACE) and routine 2D sequences. *Skeletal Radiol* 46:7–15
2. Chan WP, Lang P, Chieng PU, Davison PA, Huang SC, Genant HK (1991) Three-dimensional imaging of the musculoskeletal system: an overview. *J Formos Med Assoc* 90:713–722
3. Del Grande F, Delcogliano M, Guglielmi R et al (2018) Fully automated 10-minute 3D CAIPIRINHA SPACE TSE MRI of the knee in adults: a multicenter, multireader, multifield-strength validation study. *Invest Radiol* 53:689–697
4. Del Grande F, Guggenberger R, Fritz J (2021) Rapid musculoskeletal MRI in 2021: value and optimized use of widely accessible techniques. *AJR Am J Roentgenol* 216:704–717
5. Fayad LM, Parekh VS, de Castro Luna R et al (2020) A deep learning system for synthetic knee magnetic resonance imaging: is artificial intelligence-based fat-suppressed imaging feasible? *Invest Radiol* 56(6):357–368
6. Fritz B, Bensler S, Thawait GK, Raithel E, Stern SE, Fritz J (2019) CAIPIRINHA-accelerated 10-min 3D TSE MRI of the ankle for the diagnosis of painful ankle conditions: performance evaluation in 70 patients. *Eur Radiol* 29:609–619
7. Fritz J, Ahlawat S, Fritz B et al (2019) 10-Min 3D turbo spin echo MRI of the knee in children: arthroscopy-validated accuracy for the diagnosis of internal derangement. *J Magn Reson Imaging* 49: e139–e151
8. Fritz J, Fritz B, Zhang J et al (2017) Simultaneous multislice accelerated turbo spin echo magnetic resonance imaging: comparison and combination with in-plane parallel imaging acceleration for high-resolution magnetic resonance imaging of the knee. *Invest Radiol* 52:529–537
9. Fritz J, Raithel E, Thawait GK, Gilson W, Papp DF (2016) Six-fold acceleration of high-spatial resolution 3D SPACE MRI of the knee through incoherent k-space undersampling and iterative reconstruction-first experience. *Invest Radiol* 51:400–409

10. Glaser C, D'Anastasi M, Theisen D et al (2015) Understanding 3D TSE sequences: advantages, disadvantages, and application in MSK imaging. *Semin Musculoskelet Radiol* 19:321–327
11. Kalia V, Fritz B, Johnson R, Gilson WD, Raithel E, Fritz J (2017) CAIPIRINHA accelerated SPACE enables 10-min isotropic 3D TSE MRI of the ankle for optimized visualization of curved and oblique ligaments and tendons. *Eur Radiol* 27:3652–3661
12. Ristow O, Steinbach L, Sabo G et al (2009) Isotropic 3D fast spin-echo imaging versus standard 2D imaging at 3.0 T of the knee—image quality and diagnostic performance. *Eur Radiol* 19:1263–1272
13. Shakoor D, Guermazi A, Kijowski R et al (2018) Diagnostic performance of three-dimensional MRI for depicting cartilage defects in the knee: a meta-analysis. *Radiology* 289:71–82
14. Shakoor D, Guermazi A, Kijowski R et al (2019) Cruciate ligament injuries of the knee: a meta-analysis of the diagnostic performance of 3D MRI. *J Magn Reson Imaging* 50:1545–1560
15. Klyce W, Fritz J, Ahlwat S, Thawait G, Raithel E, Lee RJ (2019) 10-minute 3D MRI in children with acute knee trauma: Arthroscopy-Based Diagnostic Accuracy For The Diagnosis Of Internal Derangement. *Orthop J Sports Med* 7:2325967119S2325900133
16. Luna R, Fritz J, Del Grande F, Ahlwat S, Fayad LM (2020) Determination of skeletal tumor extent: is an isotropic T1-weighted 3D sequence adequate? *Eur Radiol*. <https://doi.org/10.1007/s00330-020-07394-4>
17. Breuer FA, Blaimer M, Heidemann RM, Mueller MF, Griswold MA, Jakob PM (2005) Controlled aliasing in parallel imaging results in higher acceleration (CAIPIRINHA) for multi-slice imaging. *Magn Reson Med* 53:684–691
18. Zhai H, Lv Y, Kong X, Liu X, Liu D (2019) Magnetic resonance neurography appearance and diagnostic evaluation of peripheral nerve sheath tumors. *Sci Rep* 9:6939
19. Hossein J, Fariborz F, Mehrnaz R, Babak R (2019) Evaluation of diagnostic value and T2-weighted three-dimensional isotropic turbo spin-echo (3D-SPACE) image quality in comparison with T2-weighted two-dimensional turbo spin-echo (2D-TSE) sequences in lumbar spine MR imaging. *Eur J Radiol Open* 6:36–41
20. Lee S, Jee WH, Jung JY, Lee SY, Ryu KS, Ha KY (2015) MRI of the lumbar spine: comparison of 3D isotropic turbo spin-echo SPACE sequence versus conventional 2D sequences at 3.0 T. *Acta Radiol* 56:174–181
21. Zhao F, Ahlwat S, Farahani SJ et al (2014) Can MR imaging be used to predict tumor grade in soft-tissue sarcoma? *Radiology* 272:192–201
22. Ahlwat S, Morris C, Fayad LM (2016) Three-dimensional volumetric MRI with isotropic resolution: improved speed of acquisition, spatial resolution and assessment of lesion conspicuity in patients with recurrent soft tissue sarcoma. *Skeletal Radiol* 45:645–652
23. Fayad LM, Jacobs MA, Wang X, Carrino JA, Bluemke DA (2012) Musculoskeletal tumors: how to use anatomic, functional, and metabolic MR techniques. *Radiology* 265:340–356
24. Jung JY, Yoon YC, Kim HR, Choe BK, Wang JH, Jung JY (2013) Knee derangements: comparison of isotropic 3D fast spin-echo, isotropic 3D balanced fast field-echo, and conventional 2D fast spin-echo MR imaging. *Radiology* 268:802–813
25. Kijowski R, Davis KW, Woods MA et al (2009) Knee joint: comprehensive assessment with 3D isotropic resolution fast spin-echo MR imaging—diagnostic performance compared with that of conventional MR imaging at 3.0 T. *Radiology* 252:486–495
26. Yoon MA, Hong SJ, Lee KC, Lee CH (2019) Contrast-enhanced magnetic resonance imaging of pelvic bone metastases at 3.0 T: comparison between 3-dimensional t1-weighted CAIPIRINHA-VIBE sequence and 2-dimensional T1-weighted turbo spin-echo sequence. *J Comput Assist Tomogr* 43:46–50
27. Elias DA, White LM, Simpson DJ et al (2003) Osseous invasion by soft-tissue sarcoma: assessment with MR imaging. *Radiology* 229:145–152
28. Holzapfel K, Regler J, Baum T et al (2015) Local staging of soft-tissue sarcoma: emphasis on assessment of neurovascular encasement—value of MR imaging in 174 confirmed cases. *Radiology* 275:501–509
29. Reeder SB, Wintersperger BJ, Dietrich O et al (2005) Practical approaches to the evaluation of signal-to-noise ratio performance with parallel imaging: application with cardiac imaging and a 32-channel cardiac coil. *Magn Reson Med* 54:748–754
30. Wolff SD, Balaban RS (1997) Assessing contrast on MR images. *Radiology* 202:25–29
31. Landis JR, Koch GG (1977) The measurement of observer agreement for categorical data. *Biometrics* 33:159–174
32. Belloni E, Tentoni S, Puci MV et al (2020) Patient perception of musculoskeletal MR: a survey research. *Curr Med Imaging* 16:1154–1160
33. Crombé A, Marcellin PJ, Buy X et al (2019) Soft-tissue sarcomas: assessment of MRI features correlating with histologic grade and patient outcome. *Radiology* 291:710–721
34. Del Grande F, Santini F, Herzka DA et al (2014) Fat-suppression techniques for 3-T MR imaging of the musculoskeletal system. *Radiographics* 34:217–233
35. Kirchgessner T, Perlepe V, Michoux N, Larbi A, Vande Berg B (2018) Fat suppression at three-dimensional T1-weighted MR imaging of the hands: Dixon method versus CHESS technique. *Diagn Interv Imaging* 99:23–28

Publisher's note Springer Nature remains neutral with regard to jurisdictional claims in published maps and institutional affiliations.